

## **A Colorimetric Multifunctional Sensing Method for Structural-Durability-Health Monitoring Systems**

\*Sunkook Kim<sup>1)</sup> and Healin Im<sup>2)</sup>

*1), 2) School of Advanced Materials Science and Engineering, Sungkyunkwan University,  
Suwon 440-745, Korea*

*1) [seonkuk@skku.edu](mailto:seonkuk@skku.edu)*

### **ABSTRACT**

We have developed a colorimetric multifunctional phototransistors based structural durability health monitoring system. The system is composed of an array with 4 IGZO-based phototransistors, a 405-nm light source through a side-emitting optical fiber (SOF), and pH- and Cl-selective color-variable membranes. This membrane which is sandwiched between the light source and phototransistor array responds to the presence of pH or Cl, resulting in the intensity of transmitted light. Under illumination at corrosion status of concrete, pH- and Cl-selective membrane vary their color and consequent transmitted light. IGZO based phototransistor array receives lights and exhibits the variation in photocurrent. Through this unique configuration, gradual change in membrane color corresponding to the status of concrete can be extracted in non-destructive way. By separating the data-measuring elements from sensing elements, our system can examine the accurate durability signal and multi-sense more than one degradation factor. The colorimetric durability sensing system can point out novel platform for smart durability monitoring system convincing high stability, high sensitivity and multi-function.

### **1. INTRODUCTION**

Structural health monitoring systems (SHMSs) [1] have drawn a great deal of attention due to significant advancements in internet of things (IoT), wireless communication, and smart sensors. SHMSs have been widely adopted in the architectural and civil industries. In particular, an embedded smart sensor-based durability health monitoring system (DHMS) can be applied to assess the durability and maintenance of building structures, which is highlighted as a smart application in the architecture field.

---

<sup>1)</sup> Professor

<sup>2)</sup> Graduate Student

*The 2020 World Congress on  
The 2020 Structures Congress (Structures20)  
25-28, August, 2020, GECE, Seoul, Korea*

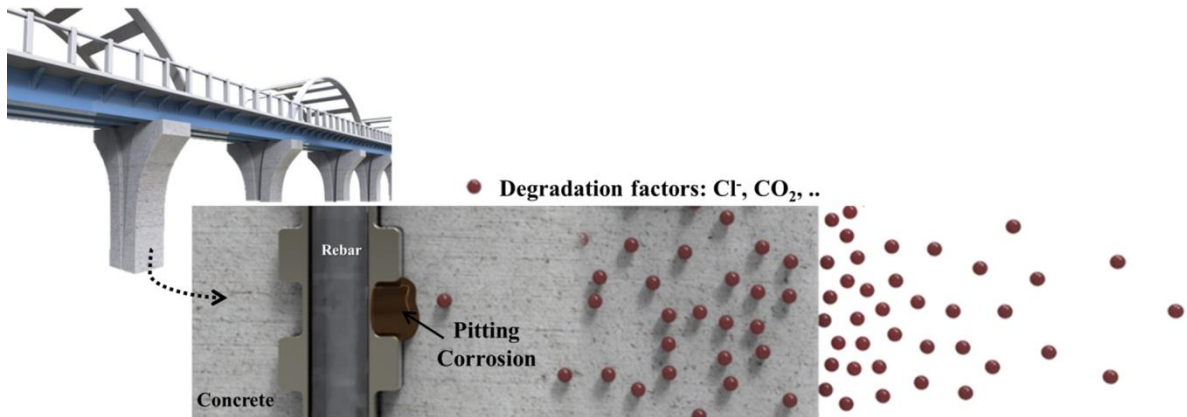
To maintain durability of building structures, condition of reinforced concrete must be monitored according to external condition while its sensors are embedded in concrete. Concrete needs to be repaired if it is degraded above threshold level through judging data obtained from embedded sensors. Each sensor node integrated into the DHMS must be operated properly inside concrete and its signal should be obtained by quantitative analysis.

There have been studies that have examined building durability, which focus on concrete corrosion [2]. According to them, during the early stages of constructing buildings, the stability of a structure remains constant. Steel corrosion may occur as time passes, which progresses from minor problems, such as strain and cracks, to major structural damage, such as cover-depth spalling and critical degradation of embedded steel. Among the various factors that contribute to deterioration, chloride attack [3] and carbonation [4] are main factors to cause significant damage in building structures. Free chloride ions in concrete cause pitting corrosion, which destroys the passivation layer on the surface of steel. Carbonation is a condition in which the pH of the concrete is lower than 10 due to the introduction of CO<sub>2</sub>, which pitting corrosion can easily accelerate. Both chloride attack and carbonation result in reducing the lifespan and strength of buildings. Therefore, *in-situ* data regarding chloride diffusion and acidity of concrete must be acquired. In addition, both modes of deterioration are the results of molecular diffusion from the surface [5], meaning depth profiling can predict concrete corrosion. However, concrete is in high alkali condition at a pH of 12 and exposed to mechanical stress after forming process. Due to harsh condition of concrete [3], the existing sensors and their system show limitations to misestimate values even the assessment is conducted in non-destructive way [6, 7]. Therefore, we suggest a novel approach to obtain *in-situ* acidity as well as Cl concentration in concrete as a function of electrical current.

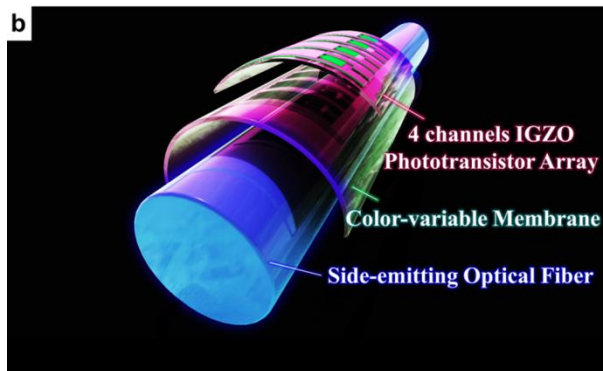
In this study, we demonstrated a colorimetric multifunctional photo-transmittance based monitoring system for durability assessment of building structures. This colorimetric system consists of an array with 4 IGZO-based phototransistors, a light source at a wavelength of 405 nm through a side-emitting optical fiber, and pH- and Cl-selective color-variable membranes. This membrane responds to the pH and the presence of Cl and shows change in its color. It is located between the light source and the phototransistor array. Under illumination with the wavelength of 405 nm at corrosion status, pH- and Cl-responsive membrane generates change in the intensity of the transmitted light, which is received by the phototransistor array as a form of electrical current [8]. Through this unique configuration of each component, gradual change in color of membrane can be extracted in a numerical way [9]. By separating the data-measuring elements from sensing elements, our system can present data regarding durability of concrete stably and accurately while monitoring more than one factor. This multifunctional colorimetric sensing system has great potential for use as a next-generation smart structure durability diagnostic tool since it demonstrates high stability [10], sensitivity [11], and density [8].

## 2. RESULTS AND DISCUSSIONS

a



b



c

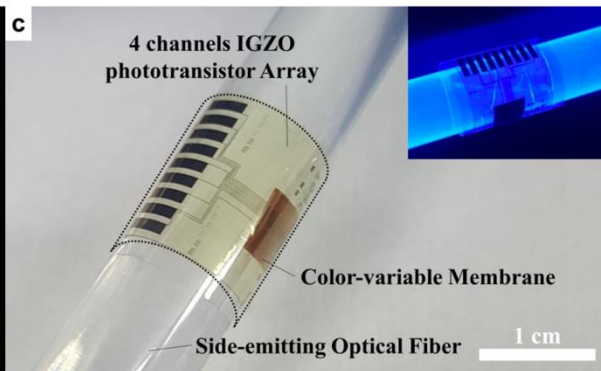


**Fig. 1** Durability assessment of building structures. a) Fundamental mechanism of corrosion progress in the concrete. b) A scheme and c) an actual image of the multifunctional colorimetric light transmittance–based durability diagnostic system.

**Fig. 1a** depicts a fundamental mechanism of corrosion progress in the concrete. Once the building is constructed, various molecules and gases penetrate the concrete surface and diffuse toward the embedded rebar. As the result of molecular diffusion from the surface, there are variations in alkalinity and chloride ion concentration along depth.

**Fig. 1b** and **1c** present a scheme and an actual image of the multifunctional colorimetric light transmittance–based durability diagnostic system for monitoring carbonation and chloride attack inside concrete. A side-emitting optical fiber (SOF) is used as a light guide and a supporting body [12], with a 405 nm laser at its edge. A color-variable membrane responds to degradation factors in its environment by changing color [13-15]. The multichannel phototransistor array consists of 4 IGZO-based phototransistors on a solution-based polyimide (PI) flexible substrate [16-18]. IGZO channels are passivated by  $\text{Al}_2\text{O}_3$  layer which prevents transistors from being influenced by chemical stress and shows high stability with less hysteresis and longer life span.

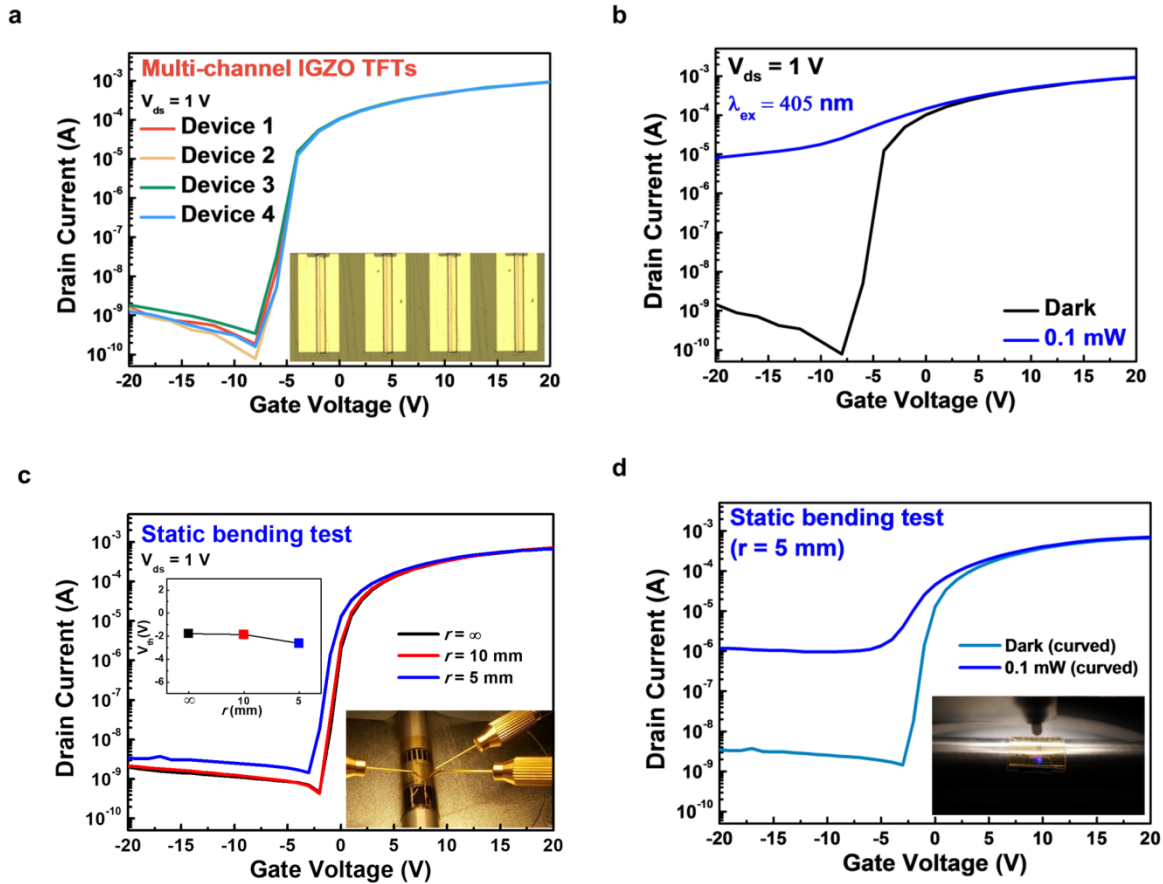


**Fig. 2** 4 IGZO channels phototransistor array. a) Transfer curves of all 4 IGZO FETs. b) Optical property of IGZO FET under light with  $P_{inc}$  of 0.1 mW at  $\lambda_{ex}$  of 405 nm. c) Static bending test of IGZO FETs with bending radii of infinity, 5 mm, and 10 mm. d) Optical property of IGZO FET bent with a bending radius of 5 mm under light with  $P_{inc}$  of 0.1 mW at  $\lambda_{ex}$  of 405 nm.

Multichannel IGZO phototransistors are required to be stable against mechanical bending stress because they should be able to operate while wrapped around SOF. Due to the solution based PI substrate's great flexibility<sup>[19,20]</sup>, the phototransistor array can remain stable on the cylindrical surface of the optical fiber along with the membrane. Prior to mechanical stability test, electrical properties of each channel are characterized in the flat condition. **Fig. 2a** shows the transfer curves of all 4 IGZO FETs in the flexible phototransistor array. It should be noted that all of the transistors exhibited substantially uniform performance with an on/off ratio ( $I_{on/off}$ ) of  $7 \pm 4 \times 10^6$  and a threshold voltage ( $V_{th}$ ) of  $-8.0 \pm 0.1$  V. The standard deviations of the  $\mu_{eff}$  and  $V_{th}$  were negligible (0.0006 and 0.11, respectively). **Fig. 2b** compares the transfer characteristics of one IGZO FET in our phototransistor array under dark and light illumination at an excitation wavelength ( $\lambda_{ex}$ ) of 405 nm with an incident optical power ( $P_{inc}$ ) of 0.1 mW. The photocurrent ( $I_{photo}$ ) was over five orders of magnitude larger than the dark current ( $I_{dark}$ ) in the off state<sup>[20]</sup>. **Fig. 2c** presents the electrical transfer characteristics of another IGZO FET in the array under statically bent conditions with bending radii of 10 mm and 5 mm (see inset of **Fig. 2c**). The statically bent condition with the bending

radius ( $r$ ) of 5 mm led to a slight negative shift in the  $V_{th}$  of the device, from -1.79 V to -2.36 V. Additionally, under the same irradiation setup in Fig. 2b, the photocurrent of the device when bent with a bending radius of 5 mm was achieved without severe degradation, as shown in Fig. 2d. For more details of the 4 IGZO phototransistors array properties, Environmental stability (Fig. S1) and uniformity characteristics (Fig. S2, Table S4) are presented in the Supporting Information.

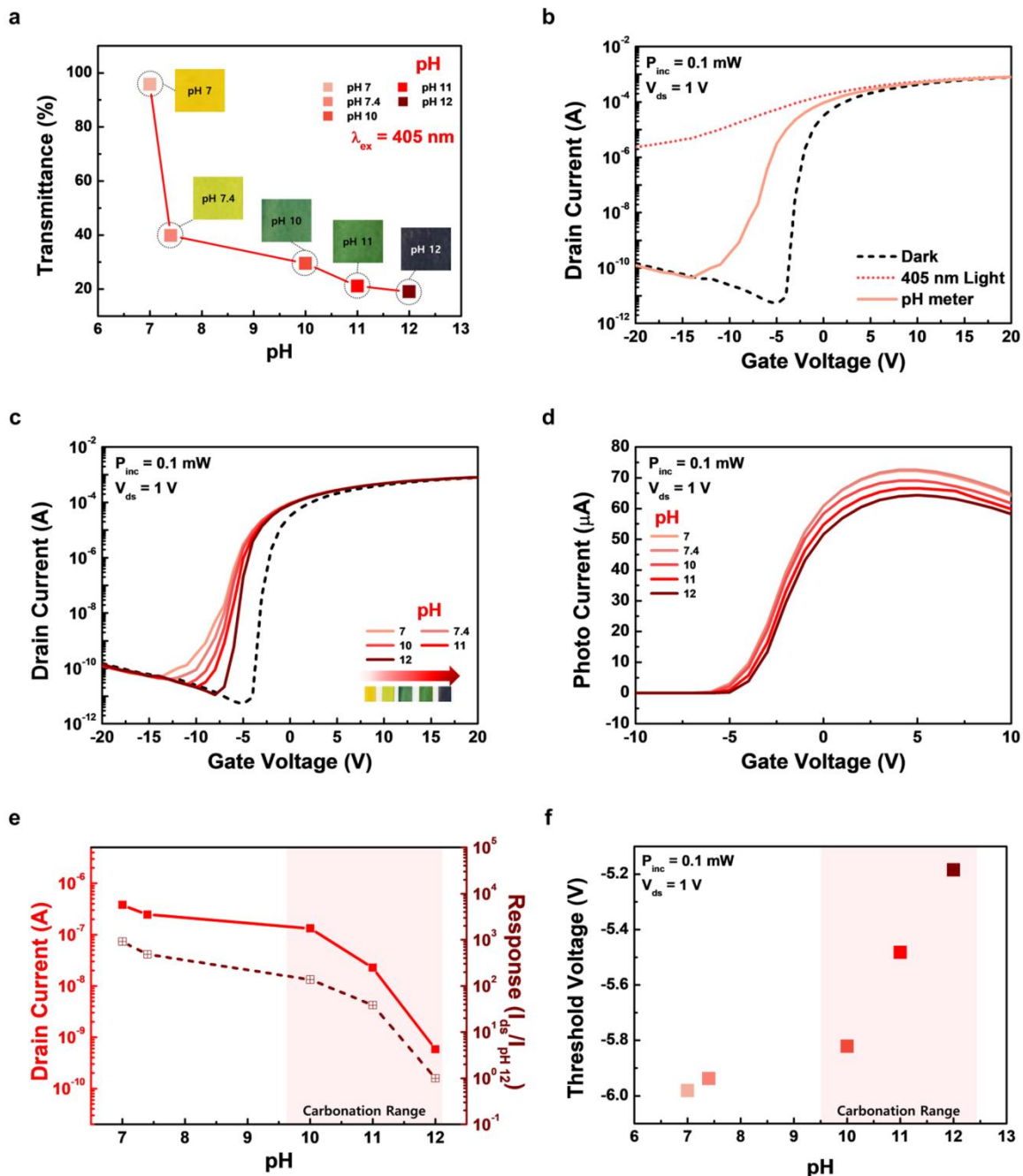


**Fig. 3** Carbonation monitoring system with pH-selective color-variable membrane (pH-membrane). a) Transmittance (%) curves at  $\lambda_{ex}$  of 405 nm depending on pH. (Inset: actual images of membrane.) b) Transfer curves of IGZO FETs w/ and w/o pH-

membrane under light with  $P_{inc}$  of 0.1 mW at  $\lambda_{ex}$  of 405 nm. c) Transfer curves and d) Photo currents of IGZO FETs w/ pH-membrane with respect to pH under light with  $P_{inc}$  of 0.1 mW at  $\lambda_{ex}$  of 405 nm. e) Drain current and response ( $I_{DS}/I_{Cl}$ ) vs pH. (f) Threshold voltage vs pH.

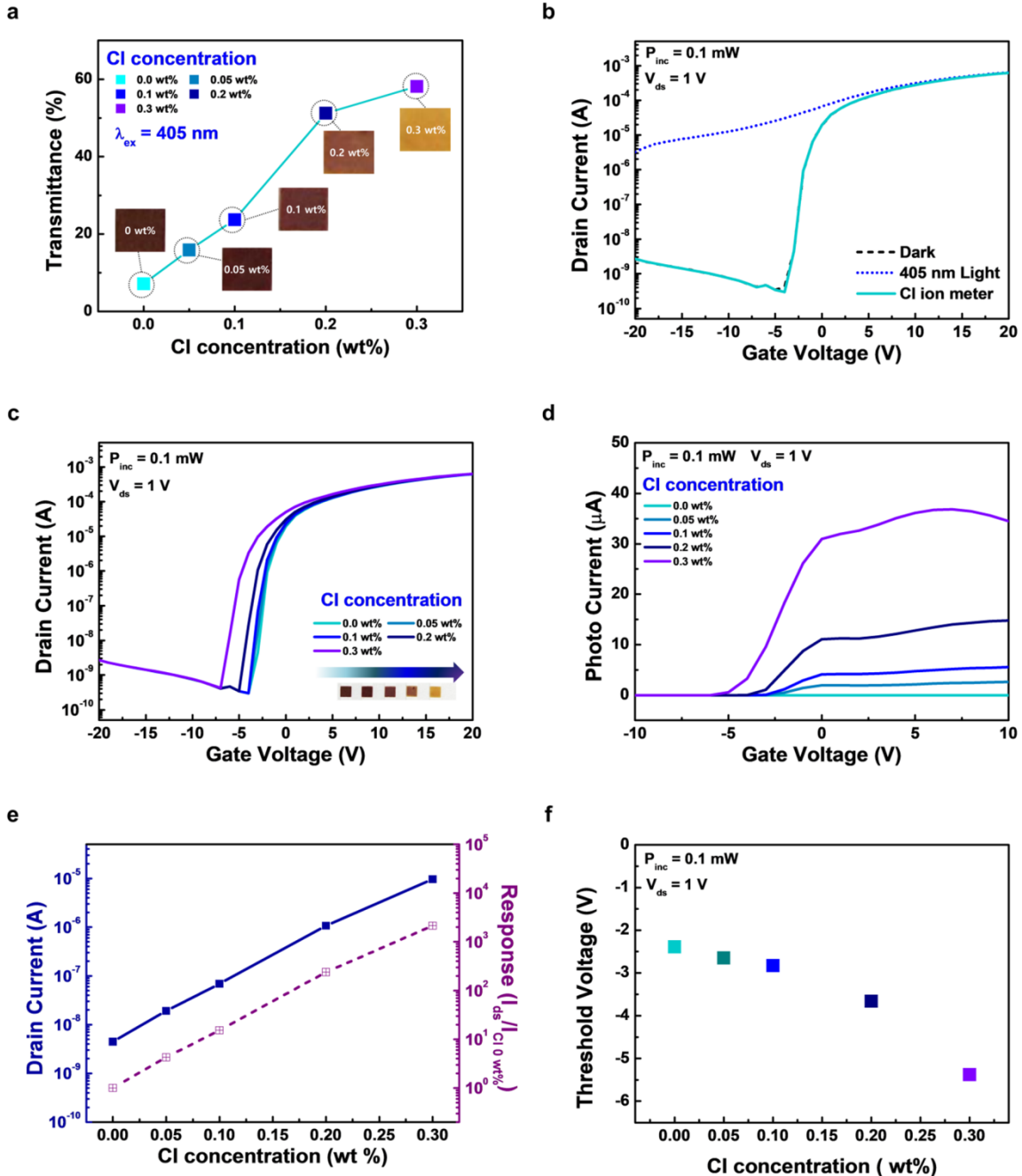


**Fig. 4 Chloride attack monitoring system with Cl-selective color-variable membrane (Cl-membrane).** a) Transmittance (%) curves  $\lambda_{ex}$  of 405 nm depending on Cl concentration (wt%). (Inset: actual images of membrane.) b) Transfer curves of IGZO FETs w/ and w/o Cl-membrane under light with  $P_{inc}$  of 0.1 mW at  $\lambda_{ex}$  of 405 nm. c) Transfer curves and d) Photocurrents of IGZO FETs w/ Cl-membrane with respect to

The 2020 World Congress on  
**The 2020 Structures Congress (Structures20)**  
 25-28, August, 2020, GECE, Seoul, Korea

Cl concentration under light with  $P_{inc}$  of 0.1 mW at  $\lambda_{ex}$  of 405 nm. e) Drain current and response ( $I/I_{Cl\ 0\ wt\%}$ ) vs Cl concentration. (f) Threshold voltage vs Cl concentration.

**Table 1.** pH-membrane transmittance (%) with pH at a wavelength of 405 nm.

pH	7	7.4	10	11	12
Transmittance [%]	95.791	39.889	29.527	21.097	19.016
Errors	0.05	0.15	0.11	0.12	0.15

**Table 2.** Cl-membrane transmittance (%) with Cl concentration at a wavelength of 405 nm.

Cl concentration [wt%]	0.00	0.05	0.10	0.20	0.30
Transmittance [%]	7.168	15.873	23.707	51.229	58.149
Errors	0.24	0.19	0.3	0.12	0.15

IGZO phototransistor with high photo-responsivity and stability [21] is applied to predict carbonation and chloride attack in concrete. **Fig. 3a** shows transmittance (%) curves of pH-selective color-variable membrane (called pH-membrane) at  $\lambda_{ex}$  of 405 nm depending on external alkalinity. As the alkalinity increases, the color membrane transitions from a yellowish-green color, below a pH of 10, to a dark green when the pH is approximately 12 (see **Fig. 3a** inset). When the pH-membrane responds at certain pH levels, the membrane shows change in color, resulting in a difference in the transmitted light intensity. As the pH increases to 10, 11 and 12, the transmittance decreases to 29.5 %, 21.1 %, and 19.0%, respectively. Therefore, transmittance of pH-membrane is inversely proportional to pH where the membrane is exposed at  $\lambda_{ex}$  of 405 nm (see **Table 1**).

**Fig. 3b** shows the  $V_{gs} - I_{ds}$  curve under 405 nm illumination on the IGZO phototransistor ( $P_{inc} = 0.1$  mW,  $V_{ds} = 1$  V). The dashed black line and the short dashed red line represent the transfer curves of the IGZO phototransistor under dark and illuminated conditions, respectively. When the sensor is irradiated without the pH-membrane, many electron-hole pairs are generated in the channel, resulting in increase

in the value of  $I_{off}$ . At  $V_{gs} = -20$  V, the value of  $I_{off}$  under light increases by nearly 250,000 times relative to the value of  $I_{off}$  in the dark due to the outstanding optoelectronic characteristics of the IGZO. However, the sensor with the pH-membrane exhibits a negative  $V_{th}$  shift with no increase in  $I_{off}$ , as shown in the **fig. 3b**. The intensity of the light transmitted through the pH-membrane drops to 0.195% compared with that of the irradiating light. Because the transmitted light possesses sufficient energy—3.06 eV, to be precise—irradiation at 405 nm generates electron-hole pairs and a negative shift in  $V_{th}$  occurs due to hole capture at photo-induced defect states (termed persistent photoconductivity (PCC)) throughout IGZO channel [7]. Therefore, photo-induced hole carriers are not sufficient to enhance  $I_{off}$  at a negative  $V_{gs}$ .

**Fig. 3c** exhibits variations in the  $V_{gs} - I_{ds}$  curves at different pH values in 405 nm light with  $P_{inc} = 0.1$  mW. In accordance with the light transmittance trends shown in **Fig. 3a**,  $V_{th}$  experiences shifts in the negative  $V_{gs}$  direction when the pH is reduced to pH of 7. This is attributed to increase in light transmittance because color of membrane becomes brighter as pH decreases. **Fig. 3d** and **3e** show the photocurrent ( $I_{photo} = I_{ds} - I_{dark}$ ) and its response ( $R = I_{ds}/I_{pH\ 12}$ ), where  $I_{pH\ 12}$  is the measured  $I_{ds}$  at a pH of 12, assuming optimal concrete condition without any carbonation.  $I_{ds}$  and  $I_{ds}/I_{pH\ 12}$  at  $V_{gs} = -7$  V exhibit a difference of  $\sim 10^3$  throughout the critical carbonation range of pH from 10 to 12. In addition, the  $V_{th}$  shift, caused by trap holes in the IGZO channel, also decreases at a pH of 12 compared to that at a pH of 10.

Like the pH-membrane, Cl-selective color-variable membrane (called Cl-membrane) shows the variation of light intensity at  $\lambda_{ex}$  of 405 nm depending on Cl concentration. **Fig. 4a** and its inset show the transmittance (%) and color measured by the Cl-membrane when the Cl wt% varies from 0.00 wt% to 0.30 wt% at  $\lambda_{ex}$  of 405 nm. As Cl concentration increases from 0.00 wt% to 0.30 wt%, the color changes from a dark reddish-brown color to a light yellow color. The variation in transmittance (%) with each Cl concentration is shown in **Table 2**.

**Fig. 4b** presents the  $V_{gs} - I_{ds}$  curve of the IGZO phototransistor under 405 nm light ( $P_{inc} = 0.1$  mW,  $V_{ds} = 1$  V). The dashed black line and the short dashed blue line represent the transfer curves of IGZO phototransistor without the Cl-membrane in the dark and under illumination, respectively. When the IGZO phototransistor with the Cl-membrane is irradiated, the transmittance of Cl-membrane is only 0.001 %, which means that the intensity of the light applied to the channel is negligible. Therefore, there is no significant photo-induced current or  $V_{th}$  shift in the phototransistor with the Cl-membrane under illumination [22]. As the Cl concentration increases, the  $V_{th}$  shifts in the negative  $V_{gs}$  direction as shown in **Fig. 4c**. The photocurrent ( $I_{photo} = I_{ds} - I_{dark}$ ) and its response ( $R = I_{ds}/I_{Cl\ 0\ wt\%}$ ), where  $I_{Cl\ 0\ wt\%}$  is the  $I_{ds}$  measured without any Cl treatment, are linearly proportional to the Cl concentration, tested at a range from 0.00 wt% to 0.30 wt%. The difference in response between the response at 0.00 wt% and 0.30 wt% is greater than  $\sim 10^3$  times, and there is an increase of nearly 50 times between each 0.05 wt% interval, as shown in **Fig. 4d** and **4e**. In addition, there is a negative shift in  $V_{th}$  shift occurs with increase in Cl concentration (see **Fig. 4f**).

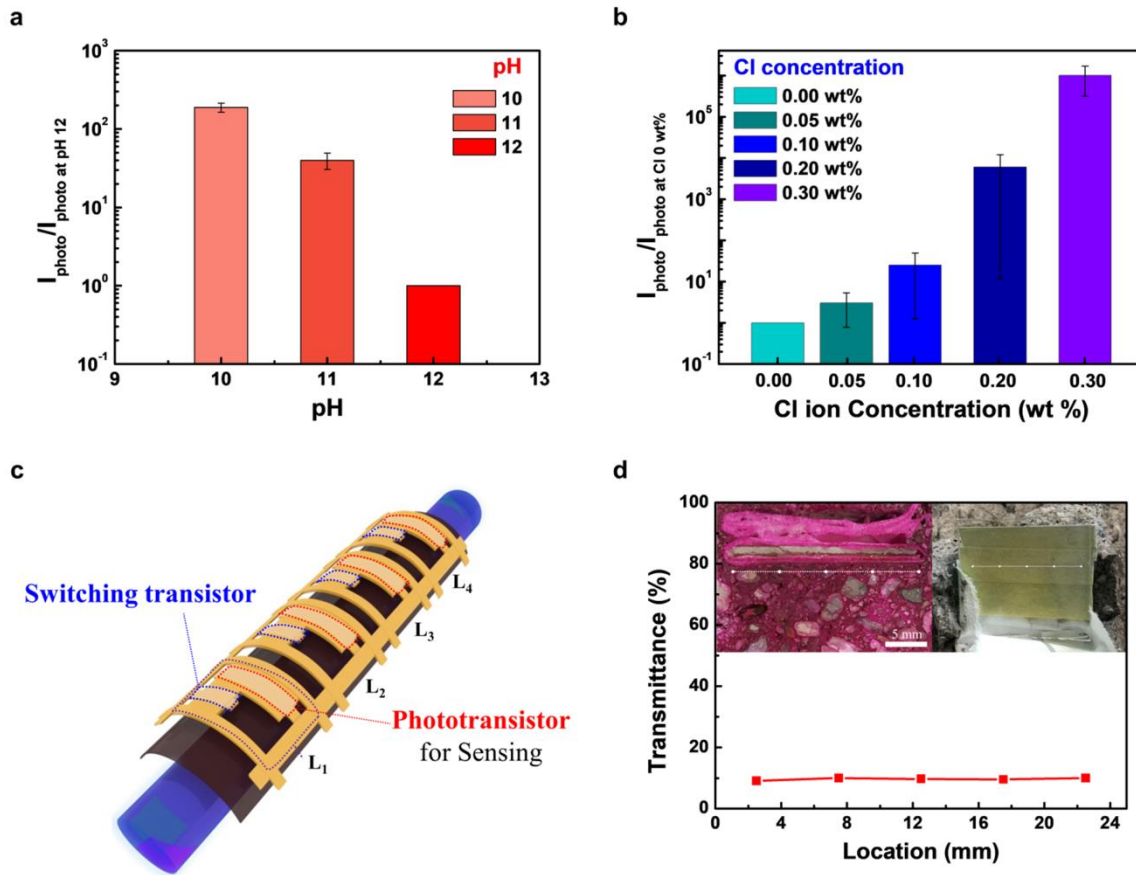


**Fig. 5 Corrosion monitoring system.** a)  $I_{photo}/I_{photo \text{ at pH } 12}$  vs pH. b)  $I_{photo}/I_{photo \text{ at Cl } 0 \text{ wt}\%}$  vs Cl concentration (wt%). c) A scheme of active matrix with phototransistors and switching transistors in series. d) Local transmittance (%) of pH-membrane embedded in mortar (Inset: (left) An actual image of mortar with phenolphthalein solution. (Right) An actual image of as-reacted pH-membrane.).

By integrating the pH-membrane and Cl-membrane with the IGZO phototransistor, we can obtain a function of the electrical signal from vital information regarding the external pH and Cl concentrations, which can examine the durability and stability in concrete for a quantitative and gradual diagnosis. **Fig. 5a** and **5b** present  $I_{photo}/I_{photo \text{ at pH } 12}$  and  $I_{photo}/I_{photo \text{ at Cl } 0 \text{ wt}\%}$  depending on the pH and Cl concentrations, respectively. If the concrete is no longer in its normal condition, the change in photocurrent ( $I_{photo}/I_{photo \text{ at normal condition}}$ , where  $I_{photo \text{ at normal condition}}$  is the photocurrent of IGZO phototransistor in where concrete is in normal states) increases, and the magnitude of this change provides numerical information on degradation of the concrete. In the case of carbonation, if concrete is in normal state,  $I_{photo}/I_{photo \text{ at pH } 12}$  is approximately 1. When carbonation occurs, the carbonation response ( $I_{photo}/I_{photo \text{ at pH } 12}$ ) increases and its value indicates degree of carbonation in quantitative way. If  $I_{photo}/I_{photo \text{ at pH } 12}$  is above  $\sim 10^2$ , the value is similar to  $I_{photo}/I_{photo \text{ at pH } 12}$  at a pH of 10 as shown in **Fig. 5a** and we can assume serious carbonation occurs. With regard to tracing chloride attack, concrete generally contains some chloride ions from the raw materials, like sand or other aggregates, and the initial Cl concentration differs between batches of concrete based

*The 2020 World Congress on  
The 2020 Structures Congress (Structures20)  
25-28, August, 2020, GECE, Seoul, Korea*

on the composition ratio of its raw materials. Therefore, the chloride concentration-dependent signal should be determined by fixing a standard initial state. For this work, Cl concentration of 0 wt% is chosen as the initial and normal state. After chloride ions diffuse into the concrete from the surface of concrete, the chloride attack response ( $I_{\text{photo}}/I_{\text{photo at Cl 0 wt\%}}$ ) begins to increase beyond its normal state value. If the Cl concentration is higher than 0.3 wt%, the chloride attack response exceeds approximately  $10^6$ .

**Fig. 5c** shows a schematic of the active matrix with 4 phototransistors and 4 switching transistors placed in series. Phototransistors are used to receive light transmittance as a function of current while switching transistors turn on and connect with phototransistors. **Fig. 5d** and inset (right) show local transmittance (%) of pH-membrane embedded in mortar with  $W/C$  of 0.5 and its real image. To confirm whether color-variable membrane actually works as an indicator and shows change in color by condition of mortar or not, pH-membrane is embedded in mortar and taken out of it after time passes enough to react the membrane with external condition. As shown in Figure 5d inset (left), due to intrinsic high alkalinity of mortar in normal state, the cross-section turns red when it is exposed to phenolphthalein solution. In accordance with phenolphthalein solution assessment, transmittance (%) at each site with an interval of 5 mm is close to 10 % and there is no significant difference among sites because of its normal condition. Therefore, this system would read depth profiling regarding corrosion behaviors differentiated from the existing methods. Furthermore, this multifunctional colorimetric optical sensing system for structural durability has a great potential to be utilized as a next-generation smart structure durability diagnostic tool with high stability, high sensitivity, and high accuracy.

### 3. CONCLUSIONS

In conclusion, we develop a multifunctional colorimetric sensing system for DHMS based on an IGZO phototransistor array with a color-variable membrane which responds to certain stimulus. The color-variable membrane is located between light source and the phototransistor array and used for sensing element to assess a pH and the presence of Cl. The membrane changes its color depending on the external condition, resulting in difference in the intensity of the transmitted light. We utilize the phototransistor array to translate gradual change in light into electrical signals such as photo-induced current ( $I_{\text{photo}}$ ),  $V_{\text{th}}$  shift, response ( $I_{\text{ds}}/I_{\text{pH 12}}$  and  $I_{\text{ds}}/I_{\text{Cl 0 wt\%}}$ ) and photocurrent variation ( $I_{\text{photo}}/I_{\text{photo at pH 12}}$  and  $I_{\text{photo}}/I_{\text{photo at Cl 0 wt\%}}$ ). On the basis of this approach, the system can be used for an active matrix with a sensor transistor and a switch transistor placed in series and a depth profiling tool to extract local information regarding durability of building structures into numerical value.

### REFERENCES

- [1] C. R. Farrar, K. Worden, *Philosophical Transactions of the Royal Society A: Mathematical, Physical and Engineering Sciences* **2007**, 365, 303.

*The 2020 World Congress on*  
**The 2020 Structures Congress (Structures20)**  
*25-28, August, 2020, GECE, Seoul, Korea*

- [2] S. Ahmad, *Cement and Concrete Composites* **2003**, 25, 459.
- [3] Y. Abbas, F. Pargar, D. A. Koleva, K. van Breugel, W. Olthuis, A. van den Berg, *Construction and Building Materials* **2018**, 174, 376.
- [4] Y. Li, S. Zhang, R. Wang, Y. Zhao, C. Men, *Construction and Building Materials* **2019**, 201, 408.
- [5] Y. Liu, R. E. Weyers, *ACI Materials Journal* **1998**, 95, 675.
- [6] H. Im, Y. Lee, D. H. Kim, O. Inturu, N. Liu, S. Lee, S. J. Kwon, H. S. Lee, S. Kim, *Construction and Building Materials* **2017**, 156, 506.
- [7] H. S. Lee, W. J. Park, H. S. Lee, S. H. Joh, *Construction and Building Materials* **2014**, 53, 403.
- [8] D. H. Kang, I. Kang, S. H. Ryu, J. Jang, *IEEE Electron Device Letters* **2011**, 32, 1385.
- [9] S. Knobelspies, A. Daus, G. Cantarella, L. Petti, N. Münzenrieder, G. Tröster, G. A. Salvatore, *Advanced Electronic Materials* **2016**, 2, 1600273.
- [10] H. D. Kim, J. H. Kim, K. Park, Y. C. Park, S. Kim, Y. J. Kim, J. Park, H. S. Kim, *ACS Applied Materials and Interfaces* **2018**, 10, 15873.
- [11] J. Kwon, Y. K. Hong, G. Han, I. Omkaram, W. Choi, S. Kim, Y. Yoon, *Advanced Materials* **2015**, 27, 2224.
- [12] G. Wandemur, D. Rodrigues, R. Allil, V. Queiroz, R. Peixoto, M. Werneck, M. Miguel, *Biosensors and Bioelectronics* **2014**, 54, 661.
- [13] M. Ornatska, E. Sharpe, D. Andreescu, S. Andreescu, *Analytical Chemistry* **2011**, 83, 4273.
- [14] A. S. Vasylevska, A. A. Karasyov, S. M. Borisov, C. Krause, *Analytical and Bioanalytical Chemistry* **2007**, 387, 2131.
- [15] A. Soni, S. K. Jha, *Biosensors and Bioelectronics* **2015**, 67, 763.
- [16] G. J. Lee, J. Kim, J. H. Kim, S. M. Jeong, J. E. Jang, J. Jeong, *Semiconductor Science and Technology* **2014**, 29, 035003.
- [17] X. F. Li, L. Y. Zhu, L. L. Chen, J. F. Shi, X. Sun, J. H. Zhang, E. L. Xin, C. C. Chen, H. C. Zang, S. T. Huo, Z. H. Ling, J. Ma, *Digest of Technical Papers - SID International Symposium* **2014**, 45, 983.
- [18] G. J. Lee, J. Kim, J. H. Kim, S. M. Jeong, J. E. Jang, J. Jeong, *Semiconductor Science and Technology* **2014**, 29, 3.
- [19] J. S. Park, T. W. Kim, D. Stryakhilev, J. S. Lee, S. G. An, Y. S. Pyo, D. B. Lee, Y. G. Mo, D. U. Jin, H. K. Chung, *Applied Physics Letters* **2009**, 95, 013503.
- [20] J. T. Jang, J. Park, B. D. Ahn, D. M. Kim, S. J. Choi, H. S. Kim, D. H. Kim, *ACS Applied Materials and Interfaces* **2015**, 7, 15570.
- [21] C. Fernandes, A. Santa, Â. Santos, P. Bahubalindrani, J. Deuermeier, R. Martins, E. Fortunato, P. Barquinha, *Advanced Electronic Materials* **2018**, 4, 1800032.
- [22] M. D. H. Chowdhury, P. Migliorato, J. Jang, *Applied Physics Letters* **2010**, 97, 173506.